Defect engineering of metal–oxide interface for proximity of photooxidation and photoreduction

Yangen Zhou[a,b,c], Zizhong Zhang[a], Zhiwei Fang[b,c], Mei Qiu[d], Lan Ling[e], Jinlin Long[a], Lu Chen[a], Yuecong Tong[a], Wenyue Su[a], Yongfan Zhang[a,d], Jeffrey C. S. Wu[f], Jean-Marie Basset[g], Xuxu Wang[a,1], and Guihua Yu[b,c,1]

[a]State Key Laboratory of Photocatalysis on Energy and Environment, Fuzhou University, Fuzhou 350002, China; [b]Materials Science and Engineering Program, The University of Texas at Austin, Austin, TX 78712; [c]Department of Mechanical Engineering, The University of Texas at Austin, Austin, TX 78712; [d]Department of Chemistry, Fuzhou University, Fuzhou 350108, China; [e]State Key Laboratory for Pollution Control and Resource Reuse, College of Environmental Science and Engineering, Tongji University, Shanghai 200092, China; [f]Department of Chemical Engineering, National Taiwan University, Taipei 10617, Taiwan; and [g]Catalysis Center, King Abdullah University of Science and Technology, Thuwal 23955-6900, Saudi Arabia

Edited by Peidong Yang, University of California, Berkeley, CA, and approved April 5, 2019 (received for review January 30, 2019)

Close proximity between different catalytic sites is crucial for accelerating or even enabling many important catalytic reactions. Photooxidation and photoreduction in photocatalysis are generally separated from each other, which arises from the hole–electron separation on photocatalyst surface. Here, we show with widely studied photocatalyst Pt/TiO_2 as a model, that concentrating abundant oxygen vacancies only at the metal–oxide interface can locate hole-driven oxidation sites in proximity to electron-driven reduction sites for triggering unusual reactions. Solar hydrogen production from aqueous-phase alcohols, whose hydrogen yield per photon is theoretically limited below 0.5 through conventional reactions, achieves an ultrahigh hydrogen yield per photon of 1.28 through the unusual reactions. We demonstrated that such defect engineering enables hole-driven CO oxidation at the Pt-TiO_2 interface to occur, which opens up room-temperature alcohol decomposition on Pt nanoparticles to H_2 and adsorbed CO, accompanying with electron-driven proton reduction on Pt to H_2.

photocatalyst | defect engineering | metal-oxide interface | solar hydrogen production | oxygen vacancy

Many catalytic reactions have two or more reaction steps and involve different active sites. The close proximity of these different active sites allows the catalytic reactions to occur or to be accelerated. For instance, many metal–oxide interfaces have highly active dual sites in many important catalytic reactions, such as Au/TiO_x, Pt/FeO_x, and Pt/FeNi$(OH)_x$ interfaces in room-temperature CO oxidation (1–3); Au/CeO_x and Au/TiO_x interfaces in water–gas shift reaction (4, 5); and Cu/ZnO_x and Cu/CeO_x interfaces in methanol synthesis (6, 7). However, the engineering of metal–oxide interfaces to create or to regulate such dual-catalytic active sites still needs insights.

In photocatalysis, holes and electrons are separated to drive oxidation and reduction independently. The close proximity between hole-driven reaction sites and electron-driven reaction sites could enable or enhance the oxidation and the reduction occur in series (8). However, this is a challenge because such close proximity could cause fast recombination of hole–electron pairs. A Schottky barrier at the metal–oxide interface can inhibit the recombination between the holes and the electrons in proximity but separated by the interface (9), which offers a possibility for the close proximity of photoreduction and photooxidation. Taking widely studied photocatalyst Pt-supported TiO_2 as a model, the holes are randomly distributed on the TiO_2 surface while the electrons are trapped on Pt nanoparticles (NPs). Therefore, locating the hole-driven reaction sites at the perimeter of the Pt NPs is a critical issue for the close proximity of photooxidation and photoreduction. High concentration of defects engineered only on the surface of photocatalysts can greatly improve photocatalytic reactions and recently triggered an explosion of research (10, 11). Such defect engineering not only changes bandgap and provides high mobility of charges but also enhances trapping of the charges by the surface (10, 12). These advantages inspire that creating a high concentration of defects only at the Pt-TiO_2 interface has promise to locate the hole-driven reaction sites at the perimeter of the Pt NPs.

Simple alcohols (methanol, ethanol, and isopropyl alcohol) represent promising hydrogen-storage materials for the future hydrogen economy, because they are liquid at room temperature, have a high gravimetric density of H_2, and can be obtained from biomass (13–15). Conventional H_2 production from these alcohols operates with heterogeneous catalysts under high temperatures (>200 °C) and high pressures (14, 15). Recently, catalyst Pt/α-MoC was reported to reduce the operation temperature to 150 to 190 °C (16). Some homogeneous catalysts have been developed for the H_2 production from methanol at 65 to 95 °C under ambient pressure (13). However, homogeneous catalysts are generally expensive, not robust enough, and difficult to be recycled. The H_2 can be produced from aqueous phase alcohols over semiconductor photocatalysts driven by solar energy under ambient condition (17). However, because electrons and holes are separated on the photocatalysts to independently drive proton reduction to H_2 and alcohol oxidation to H_2O and CO_2 in the conventional reactions, the low theoretical maximum hydrogen yield per photon (H_2/photon) of 0.5 limits the development of the solar hydrogen production from aqueous alcohols (18, 19). Moreover, it is still a huge challenge to access the hydrogen yield per photon of 0.5 for most photocatalysts so far (*SI Appendix*, Table S1).

Significance

Oxidation and reduction steps in catalysis are always in series, and excellent activity can be achieved when they occur in close proximity. Photooxidation and photoreduction are generally separated and rarely in series. This work develops defect engineering at the metal–oxide interface to make photooxidation sites close to photoreduction sites. Taking solar hydrogen production from aqueous alcohols over Pt/TiO_2 as an example, the proximity effect triggers unusual reactions and thus increases hydrogen yield per photon from 0.046 to 1.28. Our study provides a direction for the development of efficient photocatalysis.

Author contributions: Y. Zhou, X.W., and G.Y. designed research; Y. Zhou, Z.Z., M.Q., and L.C. performed research; L.L. and Y. Zhang contributed new reagents/analytic tools; Y. Zhou, Z.F., Y.T., and W.S. analyzed data; and Y. Zhou, Z.F., J.L., J.C.S.W., J.-M.B., X.W., and G.Y. wrote the paper.

The authors declare no conflict of interest.

This article is a PNAS Direct Submission.

[1]To whom correspondence may be addressed. Email: ghyu@austin.utexas.edu or xwang@fzu.edu.cn.

This article contains supporting information online at www.pnas.org/lookup/suppl/doi:10.1073/pnas.1901631116/-/DCSupplemental.

Published online May 7, 2019.

Here, the solar hydrogen production from aqueous phase alcohols over the Pt/TiO_2 is chosen to study the proximity effect of photooxidation and photoreduction. We reported that a high concentration of oxygen vacancies (V_Os) only at the Pt-TiO_2 interface can be achieved through a simple photodeposition method. This unique metal–oxide interface stabilizes not only the interfacial V_Os but also the small metallic Pt NPs. More significantly, such defect engineering makes CO oxidation at the Pt-TiO_2 interface by the holes easier to occur than direct alcohol oxidation on the TiO_2 by the holes. This relieves the blocking of active sites on the Pt by adsorbed CO, which enables continuous decomposition of alcohols on the Pt to the CO_{ads} and H_2. Meanwhile, the electrons trapped on the Pt reduce protons to H_2. These unusual reactions make the hydrogen yield per photon of solar hydrogen production from aqueous-phase alcohols reach 1.28. In this case, the alcohols no longer act as sacrificial reagents to scavenge the holes as usual but become promising hydrogen-storage materials.

Results

Solar Hydrogen Production Performance. The Pt-supported TiO_2 samples were prepared by in situ photodeposition from aqueous methanol solution containing commercial TiO_2 (Degussa P25) and chloroplatinic acid under strong UV light irradiation (125-W high-pressure mercury lamp) and Ar gas atmosphere (expressed as Pt/TiO_2-P). The H_2-production performance of the Pt/TiO_2-P photocatalysts is presented in Fig. 1*A*. For comparison, the performance of reference Pt/TiO_2-I photocatalysts, which were prepared by an impregnation–reduction method, are shown in Fig. 1*B*. When the Pt content increases from 0.1 to 1 wt %, both the Pt/TiO_2-P and the Pt/TiO_2-I samples present an increase in H_2-evolution rate. For the Pt/TiO_2-I samples, the H_2-evolution rate decreases with further increasing Pt loading, which is consistent with general results reported in the literature (9, 20). In contrast, the Pt/TiO_2-P samples show a steep increase and then a very slow decrease in the H_2-evolution rate with increasing the Pt loading from over 1 to 20 wt % (also expressed as Pt//TiO_2 below). The maximum H_2-evolution rate, which occurs at 5 wt % Pt content, is approximately 1.97 $mol \cdot g^{-1} \cdot h^{-1}$. This rate is 27 times higher than the best activity of the Pt/TiO_2-I (72.1 $mmol \cdot g^{-1} \cdot h^{-1}$). The hydrogen yield per photon of 5 wt % Pt/TiO_2-P is calculated to be 1.28 (based on photons with the wavelength below 400 nm; *SI Appendix*, Figs. S1and S2). This is not only greatly superior to the highest hydrogen yield per photon of the Pt/TiO_2-I samples (0.046) and other reported photocatalysts (*SI Appendix*, Table S1) but also breaks through the theoretical maximum hydrogen yield per photon of 0.5 based on the conventional reactions (19). The slight decline of H_2-evolution rate with increasing Pt content over 5 wt % can be explained by shading light effect of Pt NPs (a geometrical decrease of the illuminable area of TiO_2 induced by Pt NPs) (20). The controlling experiments suggest that the unusual activity of the Pt//TiO_2 sample is not affected by Cl^- ions reserved in the aqueous methanol solution or plasmonic effect of the Pt NPs (*SI Appendix*, Figs. S3 and S4). We noted that in a closed system, the H_2 is rapidly produced to have a high pressure, which gradually slows and finally stops the H_2 production (*SI Appendix*, Fig. S5). Worse than that, the activity becomes low in the second run (hydrogen yield per photon of 0.12) after removing the product H_2 by vacuuming. To avoid the high pressure of H_2, the gas products are evacuated for 5 s with a vacuum pump after every 20 min of light irradiation, and then the Pt//TiO_2 sample presents a stable high activity over at least 10 cycles of reaction/evacuation processes (Fig. 1*C*). The residual H_2 in the closed system after each evacuation process is critical for maintaining the unusual activity (*SI Appendix*, Figs. S6 and S7). When the product H_2 is completely removed by evacuation for 15 min, the H_2 production activity decreases by 75% in the second run. In the above stable cycling test, 2.94 L (at standard temperature and pressure) of H_2 evolves using 20 mg of photocatalyst and a total irradiation time of 200 min, and the corresponding turnover number reaches approximately 25,600 (based on the total number of Pt atoms). For the H_2 production from aqueous-phase ethanol and isopropanol solutions, the 5 wt % Pt//TiO_2 catalysts, which were prepared by the same in situ photodeposition method with corresponding aqueous alcohols, also have high H_2-evolution rates, close to that of H_2 production from aqueous methanol (Fig. 1*D*).

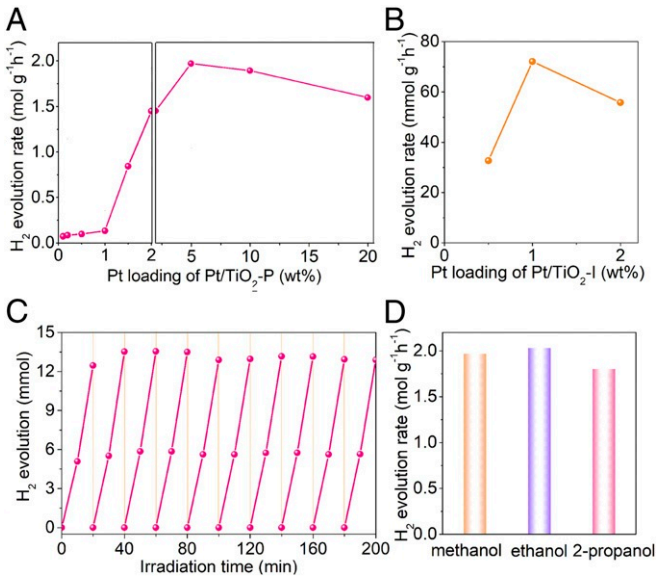

Fig. 1. Solar H_2 production performance from aqueous-phase alcohols. (*A*) Activities of Pt/TiO_2-P catalysts for H_2 production from aqueous-phase methanol under UV light irradiation. H_2-evolution rates represent the initial rates of the first half-hour. (*B*) H_2 production over Pt/TiO_2-I samples from aqueous-phase methanol under UV light irradiation, which were prepared by impregnation–reduction method. (*C*) Cycling performance of 5 wt % Pt/TiO_2 for H_2 production from aqueous-phase methanol under UV light irradiation. (*D*) H_2 production over 5 wt % Pt/TiO_2 from different aqueous-phase alcohols under UV light irradiation.

Microscopy and Spectroscopy Characterization. After drying at room temperature, the H_2-evolution rate of the Pt//TiO_2 sample is decreased by 90% (*SI Appendix*, Fig. S8), indicating the structure for the unusual activity is destroyed. Fortunately, we found that addition of a negatively charged anionic surfactant [sodium polystyrene sulfonate (PSS)] in solution to adsorb on the catalyst surface before drying can retain 55% of the unusual activity after drying at room temperature (*SI Appendix*, Figs. S8 and S9). Hence, the Pt/TiO_2-P samples with PSS protection were characterized to obtain reliable structure–activity relationship. Transmission electron microscopy (TEM) images of two typical Pt/TiO_2-P samples are shown in Fig. 2*A* and *B*. Size distributions of the Pt NPs based on a count of more than 200 individual NPs from the corresponding TEM images are represented in Fig. 2*C* (*SI Appendix*, Figs. S10–S14). The Pt NPs on the Pt/TiO_2-P samples are small with narrow size distribution. When the Pt amount increases from 0.5 to 1 wt %, the size of the Pt NPs increases from 1.1 to 2.2 nm. However, further increasing Pt loading from over 1 to 20 wt % (i.e., the Pt//TiO_2 samples) does not give rise to a significant increase in the size of the Pt NPs (maintained at approximately 2.2 to 2.6 nm). In sharp contrast, the Pt NPs on the 2 wt % Pt/TiO_2-I sample are larger (approximately 4 nm) with a wider size distribution. This phenomenon suggests that the structure on the Pt//TiO_2 samples not only allows unusual

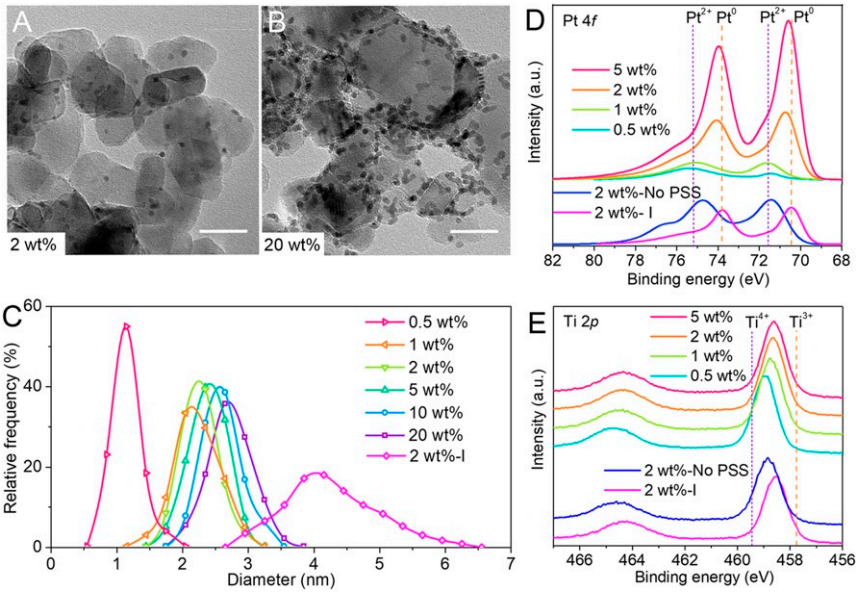

Fig. 2. Characterizations of the as-prepared Pt/TiO_2 photocatalysts. (*A* and *B*) TEM images of two typical Pt/TiO_2-P samples. (Scale bar, 20 nm.) (*C*) Particle-size distributions of Pt NPs on the Pt/TiO_2-P and Pt/TiO_2-I samples. "2 wt %-I" is the Pt/TiO_2-I sample prepared by impregnation–chemical reduction. (*D* and *E*) XPS Pt 4f and Ti 2p spectra of the Pt/TiO_2-P and Pt/TiO_2-I. "2 wt %-I" and "2 wt %-no PSS" are the 2 wt % Pt/TiO_2-I and the 2 wt % Pt/TiO_2-P that was dried without PSS protection, respectively.

activity but also provides strong adhesion between the Pt and the TiO_2 for restricting the size of the Pt NPs. We noted that the size of the Pt NPs on the 2 wt % Pt/TiO_2-P presents no change after the loss of the unusual activity caused by high H_2 pressure (*SI Appendix*, Fig. S15). This indicates that the small size of the Pt NPs is not the only key factor for the unexpected high activity of the Pt//TiO_2 samples.

The chemical states of Pt and Ti in the Pt/TiO_2 samples were investigated by X-ray photoelectron spectroscopy (XPS). As presented in Fig. 2*D*, the Pt/TiO_2-I sample shows two major peaks at 70.4 and 73.8 eV and two minor peaks at approximately 71.5 and 75.2 eV. The two major peaks are assigned to $4f_{7/2}$ and $4f_{5/2}$ of metallic Pt (Pt^0), while the two minor peaks are assigned to Pt^{2+} (21). For the Pt/TiO_2-P samples, the two samples with 0.5 and 1 wt % Pt only have Pt^{2+} species. When increasing the Pt content over 1 wt %, the Pt atoms transformation from Pt^{2+} to Pt^0. Furthermore, the sample with 5 wt % Pt mainly presents Pt^0. For comparison, the 2 wt % Pt/TiO_2-P sample without PSS protection only has Pt^{2+} species. Fig. 2*E* shows Ti XPS spectra of the photocatalysts. Standard binding energies of Ti^{4+} $2p_{3/2}$ and Ti^{3+} $2p_{3/2}$ are known to be approximately 459.5 and 457.7 eV, respectively (22). The Ti atoms in the Pt/TiO_2-P samples change from high valence (+4) toward low valence (+3), with increasing the Pt content, and stop change when the Pt loading exceeds 2 wt %. In general, the presence of $Ti^{(3+\delta)+}$ ions is indicative of V_Os in TiO_2 (23). The change in the Ti valence state suggests that the number of V_Os increases with increasing Pt content first and becomes saturated when exceeding 2 wt % Pt. In contrast, the 2 wt% Pt/TiO_2-P sample without PSS protection or after losing the unusual activity under high H_2 pressure has much fewer V_Os than the 2 wt % Pt/TiO_2-P (Fig. 2*E* and *SI Appendix*, Fig. S16). These results suggest that metallic Pt and a large number of V_Os should be crucial for the unusual activity of the Pt//TiO_2 samples and these species are easy to be oxidized. The Pt/TiO_2-I samples also have metallic Pt and abundant V_Os, but these species are stable in the air.

Oxygen Vacancies Concentrated at Pt-TiO_2 Interface. Spherical aberration-corrected scanning TEM was used to study the distribution of V_Os on the 5 wt % Pt//TiO_2. A high-resolution TEM (HRTEM) image of a typical region around the Pt-TiO_2 interface is shown in Fig. 3*A*. Fig. 3*B* shows Ti L-edge electron energy-loss spectra (EELS), which were obtained by focusing an electron beam on a region of the TiO_2 near or far away from the Pt-TiO_2 interface (labeled 1 and 2 in Fig. 3*A*, respectively). The energy-loss position of the peak is sensitive to the valence of Ti (24, 25). The signal of Ti edge from the region near the interface

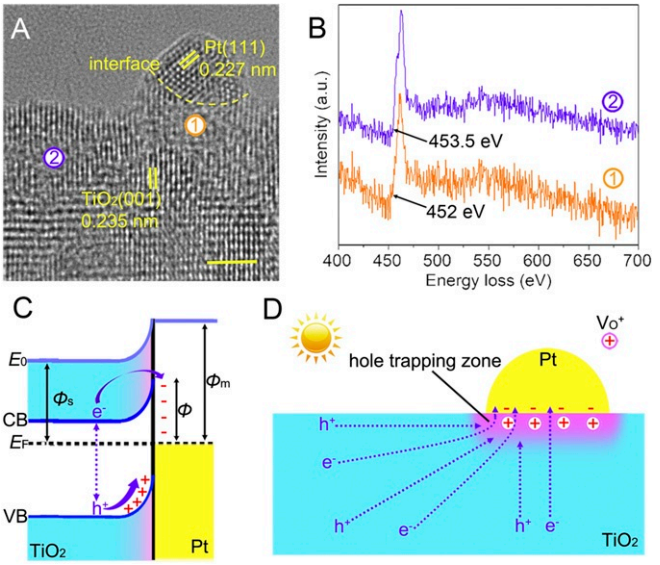

Fig. 3. Localization of oxygen vacancies at the Pt-TiO_2 interface. (*A*) HRTEM image of 5 wt % Pt/TiO_2 catalyst. (*B*) Ti L-edge EELS of TiO_2 substrate near the interface (1, yellow line) and far away from the interface (2, blue line) in *A*. (*C*) Energy diagram of the Pt/TiO_2 with oxygen vacancies concentrated at the interface. E_F, ϕ, ϕ_s, and ϕ_m are the Fermi level, the height of Schottky barrier, the work function of metal, and the work function of TiO_2, respectively. (*D*) Scheme for trapping of photogenerated charges after concentrating oxygen vacancies only at the Pt-TiO_2 interface.

at 452 eV is lower than that from the region far away from the interface at 453.5 eV, indicating lower-valence Ti species at the Pt-TiO_2 interface. The ratio between Ti^{3+} and Ti^{4+} can be estimated from the Ti EELS spectrum using a reported method (24, 25). The region near Pt presents 62% Ti^{3+} and 38% Ti^{4+}, while the region far away from the Pt shows 26% Ti^{3+} and 74% Ti^{4+}. These results indicate high concentration of V_Os at the interface of the Pt//TiO_2 samples. In contrast, a lower concentration of V_Os is evenly distributed on the TiO_2 of the Pt/TiO_2-I (*SI Appendix*, Fig. S17).

During the photodeposition process, the holes oxidize surface-lattice oxygen atoms into free active-oxygen species [O], which leaves positively charged V_O sites (-Ti^{4+}-$V_{\ddot{O}}$-Ti^{4+}-, in Kröger–Vink notation) (26). These highly reactive V_O can trap the electrons to form more stable but still reactive neutral V_Os (-Ti^{4+}-$V_O^{\times}$-Ti^{4+}-) or be healed directly by H_2O. Owing to alcohols as the scavenger for [O], anaerobic reaction system and high light flux, a large number of V_Os can be created on the TiO_2 surface (see *SI Appendix*, *Note 1*). Model study using scanning tunneling microscopy and theoretical analysis with density-functional theory (DFT) calculations have predicted size-confinement effect in noble metal NPs grown on TiO_2 with a high concentration of surface V_Os (27, 28). This can be explained in that the noble metal such as Pt with high work function is a strong electron acceptor and thus would preferentially deposit on the reactive V_Os to form relatively stable surface species with lower surface energy (26). When the Pt loading is low ($\leq$1 wt % here), the Pt particles grow to a big size with increasing the Pt loading, because reducing the high surface energy of the ultrasmall Pt particles is favored. When the Pt particles are big enough to have a small surface energy (2.6 nm here), the number rather than the size of the Pt particles increases with increasing the Pt loading, which can effectively reduce the total surface energy via covering more surface reactive V_Os. As shown in Fig. 3*C*, the Fermi level of TiO_2 is higher than the work function of Pt and thus electrons transfer from the TiO_2 to the Pt for aligning the Fermi levels (9). As a result, high Schottky barrier forms at the Pt-TiO_2 interface, which prevent electron–hole recombination but also limit electron injection to the Pt NPs. It has been reported that engineering high concentration of V_Os at the Pt-TiO_2 interface can lower the Schottky barrier height for improving the electron injection (29). Moreover, first-principles calculations reveal that the electron injection at the Pt-TiO_2 interface becomes almost ohmic-contact type for strongly reduced interfacial TiO_2 (30). Therefore, for the Pt//TiO_2, the high concentration of interfacial V_Os leads abundant electrons to transfer to the Pt, which stabilizes the V_Os and the small metallic Pt NPs. The V_Os not covered by the Pt particles will be healed by O atoms from H_2O with time (31). As a result, a large number of V_Os only exists at the Pt-TiO_2 interface of the Pt//TiO_2 samples.

The engineering of high concentration of V_Os at the Pt-TiO_2 interface for the unusual activity can be further verified by control experiments and reported results. (*i*) When the photodeposition of Pt/TiO_2-P was performed under weak UV light or in the absence of alcohols, the unusual activity was not observed (*SI Appendix*, Figs. S18 and S19). (*ii*) When dissolved oxygen in solution was not removed for the photodeposition, the unexpected high activity was also not achieved (*SI Appendix*, Fig. S20), because the V_Os could be fast-quenched by O_2. (*iii*) Comparing four different commercial TiO_2 samples, we found a positive correlation between the number of V_Os created on TiO_2 during the photodeposition process and the unusual activity of the Pt//TiO_2 sample when the number of V_Os is large enough (*SI Appendix*, Figs. S21–S24). (*iv*) Although the photodeposition method has been widely studied in the past over 40 y (20, 32), it failed to achieve the unusual activity (*SI Appendix*, Table S1). In most cases, the obtained Pt/TiO_2 samples were dried before the test, which could induce the oxidiation of the metallic Pt NPs and the V_Os. In situ photodeposition with both strong UV light and efficient scavenger has been used by many researchers (33), but the Pt loading was low (not higher than 1 wt %). (*v*) When the Pt/TiO_2 was prepared by impregnation–reduction, the $[PtCl_6]^{-2}$ is easier to be reduced than the TiO_2, due to the higher redox potential of $[PtCl_6]^{-2}/Pt^0$ (+0.744 V) than that of TiO_2/Ti^{3+} (−0.56 V). Thus, the V_Os on the TiO_2 from the chemical reduction or H_2 reduction are not the nucleation centers for the Pt deposition. Therefore, the Pt/TiO_2 from impregnation–reduction methods cannot have the unusual activity (*SI Appendix*, Figs. S25 and S26). (*vi*) The interfacial V_O-induced electron transfer from the TiO_2 to the Pt leaves positive charges on the TiO_2, which would make open-circuit potentials of the Pt/TiO_2-P samples in electrolyte shift positively in the dark (*SI Appendix*, Figs. S27 and S28). The degree of the positive shift with increasing the Pt loading is consistent with the change in the number of V_Os indicated by the XPS. Owing to the low Schottky barrier height in the Pt//TiO_2, not only are the electrons easier to be trapped by the Pt NPs, but also the holes would be attracted toward the perimeter of the Pt NPs for the charge balance (Fig. 3*D*) (29).

Proximity Effect of Oxidation and Reduction. Over the conventional Pt/TiO_2, the alcohols as sacrificial reagents are directly oxidized by the holes randomly distributed on the TiO_2 surface, while protons are reduced to H_2 by the electrons trapped on the Pt (*SI Appendix*, *Note 2*). In this case, the hydrogen yield per photon is below the theoretical maximum value of 0.5. In contrast, over the Pt//TiO_2 samples, the holes could be trapped at the periphery of the Pt NPs close to the electrons trapped on the Pt NPs. This feature was confirmed by photooxidation deposition of PbO_2, which is widely used to locate the hole-driven oxidation sites (*SI Appendix*, Fig. S29). Furthermore, the high hydrogen yield per photon of 1.28 inspires an unusual reaction mechanism, as presented in Fig. 4*A*. Dissociative adsorption of methanol into H_{ads} and CO_{ads} on Pt NPs can occur at room temperature (step 1) (34). The H_{ads} atoms can desorb as H_2 (step 2), but the adsorbed CO_{ads} molecules poison active sites of the Pt particles (35) and thus stop the further dissociative adsorption of methanol to produce H_2. When the TiO_2 is excited by photons to generate holes and electrons (step 3), the holes are trapped around the Pt-TiO_2 interface and generate hydroxyl radical ·OH to oxidize the adjacent CO_{ads} on the Pt NPs into CO_2 (steps 4 and 5). In this process, the CO_{ads} would be oxidized by one ·OH into ·COOH, and then ·COOH is oxidized by another ·OH into CO_2 and H_2O, as revealed by the previous theoretical study (36). The holes scavenge the CO_{ads} on the Pt NPs and thus enable continuous dissociative adsorption of alcohols to release H_2 on the Pt NPs at room temperature. The electrons trapped on the Pt NPs reduce protons into H_2 (step 6). So, the H_2 can be produced not only from the proton reduction but also from the alcohol dissociative adsorption, which increases the theoretical maximum hydrogen yield per photon to 1.5 (Fig. 4). In this way, the alcohols become promising hydrogen storage materials. Accordingly, the apparent quantum efficiency (AQE) of the best Pt//TiO_2 samples reaches 89.2%. In contrast, the AQE of the best Pt/TiO_2-I is only 4.9%. These results confirm the decrease in Schottky barrier on the Pt//TiO_2 can greatly enhance charge separation in photocatalytic reactions.

For the conventional Pt/TiO_2, water is the main proton source for the H_2 production, because dissociation of H_2O is much easier than that of alcohol. In contrast, for the Pt//TiO_2, the H atoms in the product H_2 should come from the protons and the alcohols (Fig. 4*A*). An isotopic tracing technique was used to verify such difference. Fig. 4*B* is the mass spectra of products H_2, deuterium hydride (HD), and deuterium (D_2) during the H_2 production

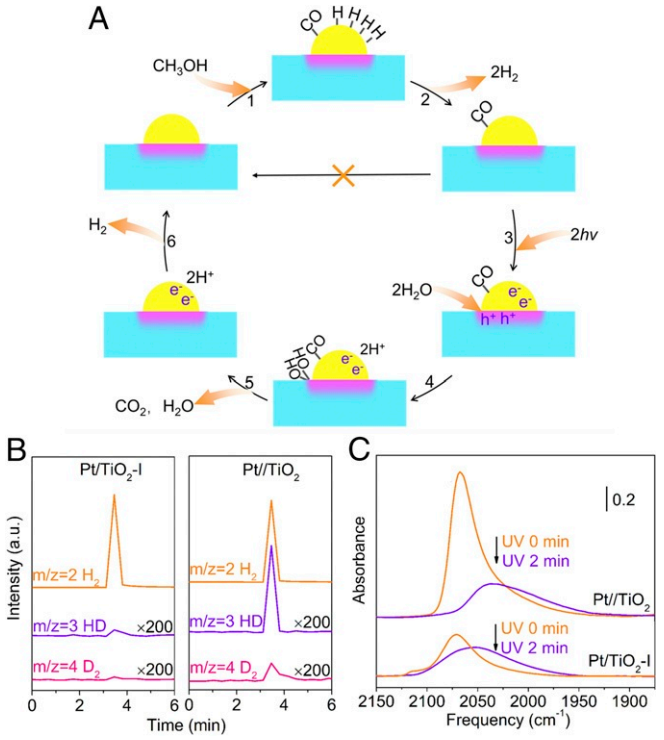

Fig. 4. Validation of the mechanism. (*A*) Unique interface-triggered photocatalytic cycle. (*B*) Mass spectra analysis of product H_2, HD, and D_2 species from solar hydrogen production from methanol solution containing CD_3OD over Pt/TiO_2-I and Pt//TiO_2. (*C*) Time-dependent IR spectra of CO adsorbed on Pt//TiO_2 and Pt/TiO_2-I during UV light irradiation.

from aqueous methanol containing deuterated methanol (84 mL CH_3OH + 1 mL CD_3OD + 85 mL H_2O) under UV light irradiation. Only trace HD and D_2 are detected for the Pt/TiO_2-I, which agrees with the literature result for the common Pt/TiO_2 (18). In contrast, for the Pt//TiO_2, a relatively large amount of HD and D_2 are detected and the ratio of HD to H_2 is much higher than that for the Pt/TiO_2-I. This evidences that H_2 production from aqueous methanol over the Pt//TiO_2 is through the proposed unusual reactions.

Fig. 4*C* displays in situ FTIR spectra of CO adsorption experiments on the Pt//TiO_2 and the Pt/TiO_2-I. The band at approximately 2,068 cm^{-1} is observed for both samples, which is attributed to the linear adsorption of CO on the Pt (37). The Pt//TiO_2 presents a much stronger CO peak than the Pt/TiO_2-I, indicating greater adsorption capacity on the Pt//TiO_2. This is due to the smaller size and larger number of the Pt NPs on the Pt//TiO_2. After 2 min of UV light irradiation, the CO peak shift to a lower wavenumber for both samples, which indicates the trapping of photogenerated electrons on the Pt (37). Interestingly, the integrated area of the CO peak decreases by 60% for the Pt//TiO_2 and remains almost unchanged for the Pt/TiO_2-I. This result reveals that the holes on the Pt//TiO_2 are trapped near the Pt NPs, which allows oxidation of the CO adsorbed on the Pt (i.e., steps 4 to 5). This feature can be further evidenced by the fact that the formation of trace byproduct CO gas during the solar H_2 production from aqueous alcohols over the Pt//TiO_2 is effectively suppressed (*SI Appendix*, Fig. S30).

DFT Calculations. To theoretically understand the oxygen-vacancy engineering at the Pt-TiO_2 interface for the proximity effect of oxidation and reduction, DFT calculations were carried out with Pt_8 cluster on anatase TiO_2 (101). Fig. 5*A* shows the most stable structures of Pt_8/TiO_2 (101) and Pt_8//TiO_2 (101) with aV_O at the Pt-TiO_2 interface. The V_O at the Pt-TiO_2 interface strengthens the bonding between the Pt_8 and the TiO_2 by 0.95 eV, which explains the restricted size and distribution of the Pt NPs on the Pt//TiO_2 (27). As shown in Fig. 5 *B* and *C*, after confining a V_O at the interface between the Pt_8 and the TiO_2 (101), the enthalpy change of the interfacial CO_{ads} + OH_{ads} reaction at the $Pt_8 - TiO_2$ (101) interface is dramatically decreased from 1.92 to −0.76 eV. This result suggests that adding V_Os at the Pt-TiO_2 interface can decrease the activation energy of CO oxidation at the Pt-TiO_2 interface, which favors the scavenging of CO adsorbed on the Pt NPs by the adjacent holes.

Conclusion

In summary, with Pt/TiO_2 as a model, we reported concentrating V_Os only at the metal–oxide interface to form hole-driven reaction sites at the perimeter of metal NPs, with the metal NPs trapping electrons for reduction. This close proximity between the photooxidation and the photoreduction triggers unusual reactions for solar hydrogen production from aqueous alcohols, which achieves an ultrahigh hydrogen yield per photon and changes the role of alcohols from sacrificial reagents to promising hydrogen storage materials. This work presents a promising strategy for synergy of photocatalytic reactions and thermocatalytic reactions. Moreover, similar to photocatalysis, catalytic redox reactions over heterogeneous catalysts always involve holes and electrons (38). Hence, this work can share insights with thermocatalytic reactions.

Materials and Methods

Both in situ photodeposition and solar hydrogen production from aqueous alcohols were performed in a closed gas-recirculation system equipped with an inner irradiation quartz reaction cell and a 125-W high-pressure mercury lamp. Typically, 20 mg of photocatalyst was added into the reactor with 170 mL of methanol solution (50 vol % methanol–50 vol % H_2O). For the in situ photodeposition process, a certain amount of H_2PtCl_6 was added. The reaction system was evacuated by a mechanical pump and then

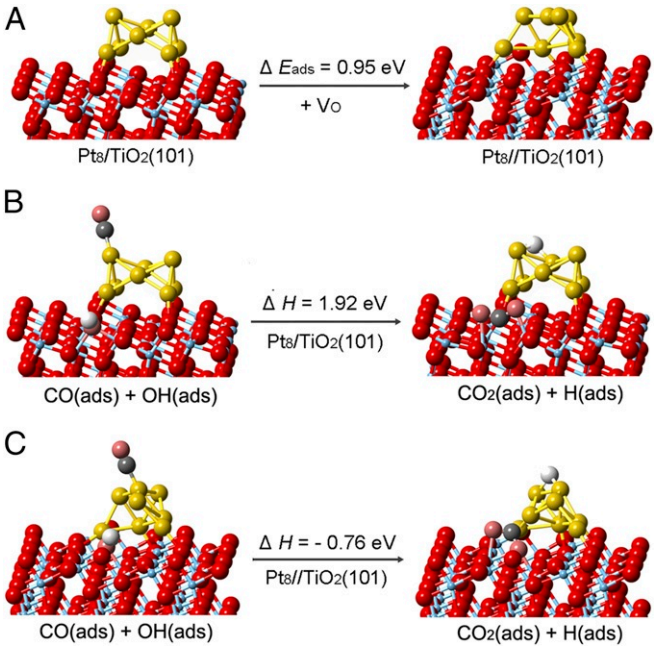

Fig. 5. Energy changes from DFT calculation. (*A*) Effect of interface V_O on the adsorption energy (E_{ads}) of Pt_8 on anatase TiO_2 (101) surface. (*B* and *C*) Energies of interfacial CO_{ads} + OH_{ads} reaction over Pt_8/TiO_2(101) and Pt_8//TiO_2(101) with V_O at the interface. Pt is in yellow, O in red or pink, Ti in blue, C in black, and H in white.

filled with 1 atm of high-purity Ar (>99.99%). This evacuation-filling process was repeated three times to remove O_2 from the system completely. Finally, 1 atm of Ar was kept in the system. During the reaction, the gas in the system was circulated with a microdiaphragm gas pump. The temperature of the solution was controlled at 10 °C by circulating water during the reaction. The product gases were determined by an online gas chromatograph.

The Pt/TiO_2-I catalysts were prepared by an impregnation–reduction method. In detail, the TiO_2 particles were impregnated with $H_2PtCl_6 \cdot 6H_2O$ solutions, dried at 120 °C, and then reduced with 0.1 M $NaBH_4$ solution.

The DFT calculations were carried out using the Vienna ab initio simulation package and the projected augmented wave method. The generalized gradient-approximation Perdew–Burke–Ernzerhof exchange-correlation functional was used.

For a complete set of detailed materials and methods, see *SI Appendix*.

ACKNOWLEDGMENTS. X.W., Y. Zhang, and W.S. acknowledge financial support from National Natural Science Foundation of China Grants U1305242, 21173044, 21373048, and 21373050. G.Y. acknowledges support from Welch Foundation Award F-1861 and the Sloan Research Foundation.

1. Chen MS, Goodman DW (2004) The structure of catalytically active gold on titania. *Science* 306:252–255.
2. Fu Q, et al. (2010) Interface-confined ferrous centers for catalytic oxidation. *Science* 328:1141–1144.
3. Chen G, et al. (2014) Interfacial effects in iron-nickel hydroxide-platinum nanoparticles enhance catalytic oxidation. *Science* 344:495–499.
4. Rodriguez JA, et al. (2007) Activity of CeO_x and TiO_x nanoparticles grown on Au(111) in the water-gas shift reaction. *Science* 318:1757–1760.
5. Fu Q, Saltsburg H, Flytzani-Stephanopoulos M (2003) Active nonmetallic Au and Pt species on ceria-based water-gas shift catalysts. *Science* 301:935–938.
6. Behrens M, et al. (2012) The active site of methanol synthesis over Cu/ZnO/Al_2O_3 industrial catalysts. *Science* 336:893–897.
7. Graciani J, et al. (2014) Highly active copper-ceria and copper-ceria-titania catalysts for methanol synthesis from CO_2. *Science* 345:546–550.
8. Wu X, et al. (2018) Solar energy-driven lignin-first approach to full utilization of lignocellulosic biomass under mild conditions. *Nat Catal* 1:772–780.
9. Linsebigler AL, Lu G, Yates JT (1995) Photocatalysis on TiO_2 surfaces: Principles, mechanisms, and selected results. *Chem Rev* 95:735–758.
10. Chen X, Liu L, Huang F (2015) Black titanium dioxide (TiO_2) nanomaterials. *Chem Soc Rev* 44:1861–1885.
11. Chen X, Liu L, Yu PY, Mao SS (2011) Increasing solar absorption for photocatalysis with black hydrogenated titanium dioxide nanocrystals. *Science* 331:746–750.
12. Zhou Y, et al. (2017) Highly efficient photoelectrochemical water splitting from hierarchical WO_3/$BiVO_4$ nanoporous sphere arrays. *Nano Lett* 17:8012–8017.
13. Nielsen M, et al. (2013) Low-temperature aqueous-phase methanol dehydrogenation to hydrogen and carbon dioxide. *Nature* 495:85–89.
14. Cortright RD, Davda RR, Dumesic JA (2002) Hydrogen from catalytic reforming of biomass-derived hydrocarbons in liquid water. *Nature* 418:964–967.
15. Deluga GA, Salge JR, Schmidt LD, Verykios XE (2004) Renewable hydrogen from ethanol by autothermal reforming. *Science* 303:993–997.
16. Lin L, et al. (2017) Low-temperature hydrogen production from water and methanol using Pt/α-MoC catalysts. *Nature* 544:80–83.
17. Chen X, Shen S, Guo L, Mao SS (2010) Semiconductor-based photocatalytic hydrogen generation. *Chem Rev* 110:6503–6570.
18. Kandiel TA, Ivanova I, Bahnemann DW (2014) Long-term investigation of the photocatalytic hydrogen production on platinized TiO_2: An isotopic study. *Energy Environ Sci* 7:1420–1425.
19. Strataki N, Bekiari V, Kondarides DI, Lianos P (2007) Hydrogen production by photocatalytic alcohol reforming employing highly efficient nanocrystalline titania films. *Appl Catal B Environ* 77:184–189.
20. Fu X, et al. (2008) Photocatalytic reforming of biomass: A systematic study of hydrogen evolution from glucose solution. *Int J Hydrogen Energ* 33:6484–6491.
21. Maeda K, Higashi M, Lu D, Abe R, Domen K (2010) Efficient nonsacrificial water splitting through two-step photoexcitation by visible light using a modified oxynitride as a hydrogen evolution photocatalyst. *J Am Chem Soc* 132:5858–5868.
22. Zhang Y-G, Ma LL, Li JL, Yu Y (2007) In situ Fenton reagent generated from TiO_2/Cu_2O composite film: A new way to utilize TiO_2 under visible light irradiation. *Environ Sci Technol* 41:6264–6269.
23. Jiang X, et al. (2012) Characterization of oxygen vacancy associates within hydrogenated TiO_2: A positron annihilation study. *J Phys Chem C* 116:22619–22624.
24. Stoyanov E, Langenhorst F, Steinle-Neumann G (2007) The effect of valence state and site geometry on Ti L3,2 and O K electron energy-loss spectra of Ti_xO_y phases. *Am Mineral* 92:577–586.
25. Matsubu JC, et al. (2016) Adsorbate-mediated strong metal-support interactions in oxide-supported rh catalysts. *Nat Chem* 9:120–127.
26. Pan X, Yang M-Q, Fu X, Zhang N, Xu Y-J (2013) Defective TiO_2 with oxygen vacancies: Synthesis, properties and photocatalytic applications. *Nanoscale* 5:3601–3614.
27. Lopez N, et al. (2004) The adhesion and shape of nanosized Au particles in a Au/TiO_2 catalyst. *J Catal* 225:86–94.
28. Wahlström E, et al. (2003) Bonding of gold nanoclusters to oxygen vacancies on rutile TiO_2(110). *Phys Rev Lett* 90:026101.
29. Yang JJ, et al. (2008) Memristive switching mechanism for metal/oxide/metal nanodevices. *Nat Nanotechnol* 3:429–433.
30. Tamura T, Ishibashi S, Terakura K, Weng H (2009) First-principles study of the rectifying properties of Pt/TiO_2 interface. *Phys Rev B*, 80:195302.
31. Wang R, et al. (1997) Light-induced amphiphilic surfaces. *Nature* 388:431–432.
32. Kraeutler B, Bard AJ (1978) Heterogeneous photocatalytic preparation of supported catalysts. photodeposition of platinum on titanium dioxide powder and other substrates. *J Am Chem Soc* 100:4317–4318.
33. Xu Q, et al. (2011) Enhancing hydrogen production activity and suppressing CO formation from photocatalytic biomass reforming on Pt/TiO_2 by optimizing anatase-rutile phase structure. *J Catal* 278:329–335.
34. Sexton BA (1981) Methanol decomposition on platinum (111). *Surf Sci* 102:271–281.
35. Bowker M, et al. (2003) Catalysis at the metal-support interface: Exemplified by the photocatalytic reforming of methanol on Pd/TiO_2. *J Catal* 217:427–433.
36. Gong X-Q, Hu P, Raval R (2003) The catalytic role of water in CO oxidation. *J Chem Phys* 119:6324–6334.
37. Shen S, et al. (2014) Effect of Pt cocatalyst in Pt/TiO_2 studied by in situ FTIR of CO adsorption. *Chin J Catal* 35:1900–1906.
38. Zeng L, Cheng Z, Fan JA, Fan L-S, Gong J (2018) Metal oxide redox chemistry for chemical looping processes. *Nat Rev Chem* 2:349–364.